# Operando Characterization of Intermediates Produced in a Lithium-Sulfur Battery

Gorlin, Y.; Siebel, A.; Piana, M.; Huthwelker, T.; Jha, H.; Monsch, G.; Kraus, F.; Gasteiger, H.A.; Tromp, M.

**DOI**
10.1149/2.0081507jes

**Publication date**
2015

**Document Version**
Final published version

**Published in**
Journal of the Electrochemical Society

# Operando Characterization of Intermediates Produced in a Lithium-Sulfur Battery

**Yelena Gorlin,[a,b,*,z] Armin Siebel,[a,*] Michele Piana,[a,**] Thomas Huthwelker,[c] Himendra Jha,[a,**,f] Georg Monsch,[d] Florian Kraus,[d] Hubert A. Gasteiger,[a,***] and Moniek Tromp[b,e]**

[a]*Chair of Technical Electrochemistry, Department of Chemistry and Catalysis Research Center, Technische Universität München, D-85747 Garching, Germany*
[b]*Catalyst Characterization, Department of Chemistry and Catalysis Research Center, Technische Universität München, D-85747 Garching, Germany*
[c]*Paul Scherrer Institute, Swiss Light Source, Laboratory for Catalysis and Sustainable Chemistry, CH-5232 Villigen PSI, Switzerland*
[d]*Philipps-Universität Marburg, Fachbereich Chemie, 35032 Marburg, Germany*
[e]*University of Amsterdam, Van't Hoff Institute for Molecular Sciences, 1098 XH Amsterdam, The Netherlands*

One of the technological barriers to electrification of transport is the insufficient storage capacity of the Li-ion batteries on which the current electric cars are based. The lithium-sulfur (Li-S) battery is an advanced technology whose successful commercialization can lead to significant gains in the storage capacity of batteries and promote wide-spread adoption of electric vehicles. Recently, important Li-S intermediates, including polysulfides, $S_3^{\bullet-}$, and $Li_2S$, have been shown to present unique X-ray absorption near edge structure (XANES) features at the sulfur K-edge. As a result, a combination of XANES characterization with electrochemistry has the potential to contribute to the understanding of Li-S chemistry. In this study, we present an *operando* XANES cell design, benchmark its electrochemical and spectroscopic performance, and use it to track reaction intermediates during the discharge of the battery. In particular, by employing electrolyte solvents with either a high or a low dielectric constant, we investigate the influence of the solvent on the conversion of polysulfide species to $Li_2S$. Our results reveal that $Li_2S$ is already formed after ~25–30% discharge in both types of electrolyte solvents, but that further conversion of polysulfides to $Li_2S$ proceeds more rapidly in a solvent with a low dielectric constant.
 [DOI: 10.1149/2.0081507jes] All rights reserved.

Manuscript submitted November 24, 2014; revised manuscript received March 2, 2015. Published March 27, 2015.

Electric vehicles represent a promising alternative to conventional transport based on an internal combustion engine and, when combined with renewable energy sources, have the potential to decrease worldwide $CO_2$ emissions by 20–30%.[1,2] In recent years, they have been gaining popularity in the form of passenger cars, with the number of sold units surpassing the 100,000 mark in 2012.[2] One of the main technological barriers to an even wider adoption of electric cars and a complete displacement of the $CO_2$-emitting vehicles is the insufficient storage capacity of the current battery technology, which leads to a limited vehicle driving range.[2,3] The useable energy density of state-of-the-art lithium-ion batteries employed in recent electric vehicles amounts to only ≈120 $Wh/kg_{system}$,[4] which corresponds to a practical driving range of 150–200 km. If one succeeds in the development of sufficiently durable high-voltage or high-energy cathode materials and combines them with silicon anodes, an energy density of ≈250 $Wh/kg_{system}$ would be in reach.[4]

An alternative promising battery concept is the lithium-sulfur (Li-S) battery.[3,5–7] Current development in Li-S battery research includes successful commercialization of Li-S cells with 260 $Wh/kg_{system}$ energy density by Sion Power corporation.[8] This value already exceeds the DOE target for 2022 (250 $Wh/kg_{system}$)[9] and has the potential to also comply with the system cost target of 125 USD/kWh[9] because of the abundance and low cost of sulfur. To achieve even greater gains in the performance and, most importantly, to improve the cycle life of Li-S batteries, it will be necessary to gain a deeper mechanistic understanding of the 16 $e^-/S_8$ interconversion between $S_8$ and $Li_2S$ shown in reaction 1.[10]

$$S_8 + 16\,e^- + 16\,Li^+ \rightleftharpoons 8\,Li_2S \qquad [1]$$

Although the detailed intermediate (electro)chemical steps involved in reaction 1 have not yet been fully established, previous fundamental studies have identified that the initial discharge products depend on the electrolyte solvent properties.[11–14] In particular, an additional intermediate characterized as a $S_3^{\bullet-}$ (a radical anion)[15,16] has been shown to form in strongly ion-solvating environments (i.e., high dielectric solvents such as dimethyl sulfoxide, dimethylacetamide, and *N,N*-dimethylformamide), but not in poorly ion-solvating environments (i.e., low dielectric solvents such as 1,3-dioxolane, 1,2-dimethoxyethane, or their 1:1 mixture by volume).[11,14] The formation of the radical likely proceeds according to the following reactions:[13–15,17]

$$S_8 + 2\,e^- \rightarrow S_8^{2-} \qquad [2]$$

$$S_8^{2-} \rightarrow S_6^{2-} + \frac{1}{4}\,S_8 \qquad [3]$$

$$S_6^{2-} \rightleftharpoons 2\,S_3^{\cdot-} \qquad [4]$$

resulting in more than 2 $e^-/S_8$ consumed per $S_3^{\bullet-}$ generated (viz., 2.67 $e^-/S_8$ based on reactions 2–4). The earliest support for this mechanism came from the study by Bonnaterre and Cauquis, who had shown that the generated amount of $S_6^{2-}/S_3^{\bullet-}$ peaks at around 2.7 $e^-/S_8$, before being subsequently reduced to $S_4^{2-}$.[15] In contrast to the above mechanism, the initial reduction of $S_8$ to $S_4^{2-}$ in low dielectric solvents has been recently shown to proceed through a single reduction step in a rotating ring-disk electrode study.[14] Similar mechanistic understanding of the subsequent conversion of $S_4^{2-}$ to $Li_2S$ through a variety of possible reduction, disproportionation, and precipitation steps in different types of solvents has not yet been established and several competing mechanisms of $Li_2S$ formation have been proposed.

It was originally believed that $S_4^{2-}$ was first reduced to $S_2^{2-}/Li_2S_2$ and the $S_2^{2-}/Li_2S_2$ species were then subsequently reduced to $Li_2S$.[6,18,19] Based on this sequential electro-reduction mechanism, it was hypothesized that $Li_2S$ formation may be correlated with the final change in the slope of the galvanostatic discharge curve and the resulting incomplete utilization of sulfur.[18] Several recent experimental and theoretical studies, however, have demonstrated the possible for-

*Electrochemical Society Student Member.
**Electrochemical Society Active Member.
***Electrochemical Society Fellow.
[f]Present address: Atotech Deutschland GmbH, 10553 Berlin, Germany.
[z]E-mail: yelena.gorlin@tum.de

mation of $Li_2S$ early into the discharge, after only 4 $e^-/S_8$ consumed, instead of at the very end of the discharge.[20–22] Such early detection of $Li_2S$ suggests that the formation of lower order polysulfides and solid products is simultaneous and not sequential.

The observed formation of $Li_2S$ after a consumption of only 4 $e^-/S_8$ could occur either through a series of concurrent electro-reduction steps as proposed by Kumaresan and co-workers[22] or through various disproportionation steps, as proposed by Lu and co-workers.[14] Two examples of possible disproportionation steps, leading to formation of $Li_2S$ and either a higher order polysulfide or $S_8$ are shown in reactions 5 and 6.

$$Li_2S_4 \rightleftharpoons \frac{4}{7} Li_2S + \frac{3}{7} Li_2S_8 \quad [5]$$

$$Li_2S_4 \rightleftharpoons Li_2S + \frac{3}{8} S_8 \quad [6]$$

The main difficulty in the exact classification of the mechanism leading to the conversion of $S_4^{2-}$ to $Li_2S$ stems from the intractability of lower order polysulfides in cyclic voltammetry and potential-controlled half-cell studies, often referred to as short-term electrolysis tests in literature.[14,15,17] The reactions probed using these methods occur on the timescale of seconds to minutes, while the conversion of $S_4^{2-}$ to $Li_2S$ likely occurs on the timescale of minutes to hours.[14] Furthermore, standard non-electrochemical characterization techniques employed to differentiate between various reduction products during long-term half-cell tests usually can detect either solid and crystalline $Li_2S$ or liquid polysulfides, but not both solid and liquid products at the same time. For example, X-ray diffraction (XRD)[19,20] and solid-state magic angle spinning nuclear magnetic resonance (NMR) spectroscopy[23] have been previously used to successfully track $Li_2S$ formation, while ultraviolet-visible (UV-Vis) spectroscopy,[15,17,24,25] high performance liquid chromatography (HPLC),[25] and solution NMR[23,26] have been used to identify polysulfide intermediates in the electrolyte. Although some attempts have been made to extend UV-Vis spectroscopy and solution NMR techniques toward quantification of $Li_2S$, these experiments saw only limited success, because $Li_2S$ lacked unique spectral features and had poor solubility in the electrolyte.[23,24,26] Consequently, new characterization techniques are necessary to elucidate the process of $Li_2S$ formation during the discharge of Li-S batteries.

Recently, several Li-S reaction intermediates, including polysulfides,[27–29] $S_3^{\bullet-}$,[30,31] and $Li_2S$ solid product,[27,32] have been shown to present unique features in the sulfur K-edge X-ray absorption near edge structure (XANES) spectrum. As a result, sulfur K-edge XANES has the potential to contribute to the understanding of the discharge mechanism in the 4–16 $e^-/S_8$ discharge region, which is known as the low voltage plateau, and facilitate the rational design of improved Li-S batteries. Previous *operando* XANES studies have employed a pouch or a coin cell, which had been modified by an X-ray transparent window.[27,28,32–35] Such a cell design resulted in XANES spectra, which were completely governed by the sulfur electrode and the electrolyte present in its pores, because of the low penetration depth of the X-rays at the sulfur K-edge energy. The rest of the species, which were located in the electrolyte between the two electrodes, were almost invisible to spectroscopic characterization.[28] In our work, we introduce an alternative cell design, which eliminates the back side of the sulfur electrode from the path of the X-rays and enables spectroscopic characterization of all three components of the battery: the cathode, the anode, and the separator. In the experiments, we first benchmark the electrochemical performance of our cell against a standard Swagelok T-cell and then validate the ability of our cell to measure intermediates by tracking the formation of $S_3^{\bullet-}$ in a cell containing an electrolyte solvent with strong ion-solvating properties. Having established the spectro-electrochemical capabilities of our *operando* cell, we use it to characterize the low-voltage plateau intermediates in two cells containing electrolyte solvents with significantly different dielectric constants. We successfully detect the initial $Li_2S$ formation after a discharge of ~4–5 $e^-/S_8$ in both types of electrolyte solvents and identify the influence of the solvent on the subsequent transformation of polysulfides to $Li_2S$.

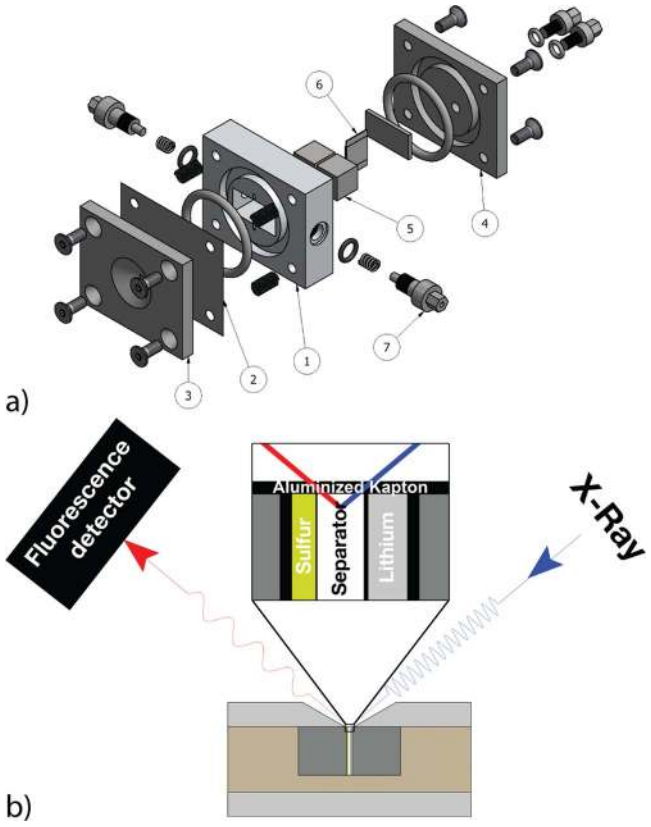


**Figure 1.** a) Exploded view of the spectro-electrochemical operando cell, depicting its individual components: 1) cell base; 2) X-ray window, aluminized Kapton; 3 and 4) aluminum front-plate and back-plate; 5) stainless-steel current collectors; 6) electrode-separator assembly; 7) stainless-steel electrical contact pins. b) Schematic of XANES setup illustrating monochromatic X-rays penetrating the cell through an aluminized Kapton window. XANES spectra are measured in fluorescence mode at 90° with respect to the incoming beam. Inset graphic shows a close-up of the electrode arrangement and measurement geometry inside the electrochemical cell (electrical contact not shown); the X-ray beam can, in principle, be micro-focused on the cathode electrode, the separator, and the anode electrode.

## Experimental Section

*Cell design.*— The *operando* cell design is presented in Figure 1a. The cell consists of a cell base (Fig. 1a, (1)) made from polyether ether ketone (PEEK), an electrical insulator, which offers good mechanical properties and is chemically inert. An 8 micron thick Kapton foil metallized with a 100 nm thick layer of aluminum (Multek, USA) is used as an X-ray window (Fig. 1a, (2)) during the XANES experiments. It proves to be an excellent air and water barrier on the time scale of hours, while offering about 50% transmission for X-rays at the sulfur K-edge at 2500 eV, when the cell is mounted at 45° relative to the beam. The foil is positioned in between the cell base and an aluminum front-plate (Fig. 1a, (3)). The front-plate has a 2 mm diameter hole, which is tapered by 50° to allow the X-rays to enter and leave the cell. Sealing of the electrolyte compartment is realized using two chemically inert Viton O-rings between the front-plate and an aluminum back-plate (Fig. 1a, (4)).

The cell base features a rectangular cut-out, open on both sides, in which the stainless-steel (DIN 1.4751) current collectors (Fig. 1a, (5)) and the electrode-separator assembly (Fig. 1a, (6)) reside. The electrical contact with the potentiostat is made through contact pins (Fig. 1a, (7)) on either side of the cell. The contact pins are compress-

ing the current collectors with a constant force of ca. 20 N via two stainless-steel springs.

A schematic of the *operando* XANES setup demonstrating the measurement geometry and cell components is shown in Figure 1b. Monochromatic, focused X-rays are entering the cell through the hole in the front window and are passing through the aluminized Kapton foil. Inside the cell, they interact with sulfur species, resulting in the emission of fluorescent X-rays. After the fluorescent X-rays leave the cell, they are registered by an energy dispersive fluorescence detector positioned at an angle of 90° with respect to the incident beam. We calculate that we can measure the X-rays that pass through approximately 10–20 μm of the electrolyte. Because the cathode and the separator are highly porous materials, they have a negligible contribution toward attenuation of the X-rays. Although in this study we have measured with a defocused beam across the sulfur electrode and the separator to minimize beam damage, the described cell design would, in principle, be able to conduct spatially-resolved XANES measurements of the cathode electrode, the separator, and the anode electrode. In these measurements the ratio of electrolyte to sulfur loading will have to be carefully considered, as it will have an influence on the equilibrium of the species that form inside the separator.

*Electrochemical measurements.*— Electrochemical measurements were performed in a standard stainless-steel T-cell made from Swagelok components and in the *operando* cell. Electrolytes were prepared from 1 M lithium perchlorate ($LiClO_4$, battery grade, 99.99% trace metal basis, Sigma-Aldrich) and 0.5 M lithium nitrate ($LiNO_3$, 99.99% trace metal basis, Sigma-Aldrich), an additive to enhance surface passivation of the Li electrode, dissolved in either a mixture of 1,3-dioxolane (DOL, anhydrous, 99.8%, Sigma-Aldrich) and 1,2-dimethoxyethane (DME, anhydrous, 99.8%, Sigma-Aldrich) (1:1 vol:vol) or *N,N*-dimethylacetamide (DMAC, anhydrous, 99.8%, Sigma-Aldrich). These solvents will be subsequently referred to as DOL-DME and DMAC, respectively. We chose $LiClO_4$ as an electrolyte salt rather than the commonly used bis(trifluoromethanesulfonyl)imide lithium (LiTFSI) in order to eliminate the additional contribution of sulfonyl group to the XANES spectrum. Preliminary experiments were also performed using 1 M LiTFSI (99.95 % trace metal basis, Aldrich) and 0.5 M $LiNO_3$ dissolved in DOL-DME in both the Swagelok T-cell and the *operando* cell to benchmark the performance of the *operando* cell and to compare the discharge behavior of the battery in the electrolytes based on $LiClO_4$ or LiTFSI salts.

The sulfur/carbon ($S_8$/C) composite was prepared by wet impregnation of 1.5 g Vulcan carbon (XC-72, Tanaka Kikinzoku Kogyo) with 120 ml of a 1 M solution of sodium thiosulfate ($Na_2S_2O_3 \cdot 5\ H_2O$, 99.5%, Sigma-Aldrich) for 10 min.[36] The wet impregnation step was followed by 20 min ultrasonic treatment after which a well-dispersed, homogeneous suspension was obtained. To this suspension an excess of 250 ml of 1 M $HNO_3$ (ACS reagent, Sigma-Aldrich) was added, and the mixture was sonicated for another 20 min. Afterwards, the supernatant was decanted, washed three times with double-distilled water, and filtered to obtain the composite. The obtained composite was dried over silica gel in a sealed glass oven (Büchi, Switzerland) at 80°C for 72 h. Finally, the composition of the material was determined to be 67 wt% sulfur by thermogravimetric analysis.

To prepare an electrode, the $S_8$/C composite was added to a suspension of polyvinylidene difluoride (PVDF HSV900, Kynar) in N-Methyl-pyrrolidinone (NMP, 99.5%, anhydrous, Sigma-Aldrich). The weight of the composite and PVDF were adjusted to give an ink composition of 85 wt% $S_8$/C composite and 15 wt% PVDF. The resulting ink was vigorously mixed for 2 h, spread onto a current collector (17 μm thick aluminum foil) using a Mayer rod with a wet-film thickness of 250 μm, and dried for 72 h. These three steps were all performed at room temperature. From the resulting coating, the cathode electrodes were punched out and determined to have a sulfur loading of $1.8 \pm 0.1$ mg/cm$^2{}_{\text{electrode}}$.

The electrochemical cells were assembled using these electrodes at the cathode and a piece of lithium metal (99.9% purity, Rockwood Lithium, USA) at the anode. The area of the electrodes was either 0.80 cm$^2$ or 0.90 cm$^2$, depending on whether they were used with the Swagelok T-cell or the *operando* cell, respectively. For the experiments in DMAC electrolyte, lithium was pre-conditioned for 24 h in propylene carbonate (PC, 99.7% purity, Aldrich) containing 1 M $LiClO_4$. Sulfur and lithium electrodes were separated by a 200 μm glass-fiber separator (Glass microfiber filter 691, VWR, Germany), which was soaked with 100 μl of the electrolyte. Due to the high sensitivity of the cell chemistry and, particularly, of the lithium metal, to air and water, all components, with the exception of $S_8$/C electrodes, were thoroughly dried at 70°C under dynamic vacuum for a minimum of 1 h before being transferred into a glove box containing less than 1 ppm of oxygen and water. $S_8$/C electrodes were dried over silica gel at 80°C to avoid sublimation of sulfur.

The assembled electrochemical cells were connected to a SP-200 single-channel potentiostat (Bio-Logic SAS, France), which was first used to record a potentio-electrochemical impedance spectrum and then to galvanostatically discharge the cell at a C-rate of 0.1 h$^{-1}$ (based on a theoretical capacity of 1672 mAh/g$_s$) to a cut-off voltage of 1.5 V vs. Li/Li$^+$. The open circuit voltage (OCV) period between the cell assembly and the beginning of the discharge was always 1–2 h.

*Sulfur K-edge XANES measurements.*— Sulfur K-edge XANES measurements were performed at the PHOENIX beamline of the Swiss Light Source (SLS, Paul Scherrer Institut, Villigen, Switzerland) and at I18 beamline of the Diamond Light Source (DLS, Didcot, UK). The initial cell was commissioned and tested at I18 beamline of the DLS, while the actual *operando* data, which is presented in this paper, were obtained at the PHOENIX beamline of the SLS. The PHOENIX beamline is a tender X-ray beamline, covering the energy range from 0.8 to 8 keV. Its optical concept closely follows the LUCIA beamline at Soleil synchrotron facility.[37] In its setup, an elliptical undulator serves as source for the X-rays. Monochromatic X-rays with an energy resolution of about 0.3 eV are generated using a Si(111) double-crystal monochromator (DCM). The beam is subsequently focused using a set of mirrors in Kirkpatrick-Baez configuration, with the maximum possible focus corresponding to a spot size of 2.5 μm × 2.5 μm. In the experiments, the *operando* cell was mounted in a large sample chamber filled with helium gas at a pressure of 750 mbar. XANES spectra were recorded at the sulfur K-edge in fluorescence mode using a 4 element Vortex detector. Data acquisition was run continuously yielding one spectrum every 8 minutes for the DOL-DME cell and one spectrum every 9 minutes for the DMAC cell. These acquisition times corresponded to an electrochemical charge increment equivalent to 0.22 and 0.24 $e^-/S_8$ (23 and 25 mAh/g$_s$), respectively. Fluorescence XANES spectra were normalized using the fluorescence signal of the aluminum window (Al $K_\alpha$ Fluorescence) as $I_0$. The acquired XANES spectra were then processed using the Athena software package.[38]

Before performing the *operando* experiments, we collected XANES spectra of an $S_8$/C composite electrode with 100 μl of the DOL-DME electrolyte containing 1 M $LiClO_4$ and 0.5 M $LiNO_3$ in a well-sealed container. As expected, in the first spectrum, only the signature of elemental sulfur was observed. Subsequent spectra recorded in the same spot, however, demonstrated an emergence of two new features at incident energies of 2482 eV and 2498 eV. The fact that these features were not present in the initial spectrum and that no electro-chemical reaction could occur inside the sealed cell, suggests that their appearance is linked to beam-induced oxidation of sulfur in the presence of the electrolyte. Comparison of the spectra with those of $Li_2SO_4$ powder identifies the produced species as sulfate (Supplemental material, Fig. S1a). The presence of beam-induced oxidation is further substantiated by the fact that the concentration of sulfate (expressed as the magnitude of the peak) is related to irradiation time and that a clean spectrum of elemental sulfur can be obtained after moving the beam to a new spot on the sample. To reduce the extent of radiation damage we defocused the beam from its initial spot size of 10 μm x 10 μm to a spot size of 1800 μm x 50 μm and reduced the flux of the incoming photons by one order of magnitude by changing to a higher harmonic of the undulator. The combination of

these measures, which resulted in a ~$10^4$-fold lower radiation flux, successfully avoided radiation-induced reactions (Supplemental material, Fig. S1b) and, ultimately, allowed continuous acquisition of XANES spectra over the course of ~7 hours. After the discharge had lasted longer than 7 hours in the DOL-DME cell, a small beam-induced feature was observed (Fig. 6), although no corresponding beam-damage was observed in the DMAC cell. One disadvantage of using a defocused beam was that it made it difficult to selectively measure the signal from either the sulfur electrode or the separator, and the XANES data presented in this study corresponds to a signal average over these two components of the battery. In our future work, we will optimize the thicknesses of the electrodes and the separator, as well as beamline configuration, to allow spatially-resolved XANES measurements in the absence of beam-induced oxidation of sulfur intermediates.

*Data analysis.*— Qualitative analysis of XANES spectra was performed using 3 powder standards: $S_8$, $Na_2S_4$, and $Li_2S$. Commercially available powders were used for $S_8$ (99.998% trace metal basis, Sigma-Aldrich) and $Li_2S$ (99.98% trace metal basis, Sigma-Aldrich). Prior to XANES characterization the powders were manually ground and diluted with cellulose to a final concentration of 10 wt%. $Na_2S_4$ polysulfide was prepared using a known literature procedure.[39] Briefly, a stoichiometric mixture of Na metal (1 mmol) and sulfur was added to approximately 0.5 ml of anhydrous ammonia in a flame-sealed bomb tube at room temperature. After a reaction time of a couple of days, the bomb tubes were cooled to −78°C and opened, the ammonia was pumped off, and $Na_2S_4$ powder was obtained. The phase purity of the powder was checked using powder-XRD and infrared spectroscopy. $Na_2S_4$ was subsequently diluted following the same procedure as $S_8$ and $Li_2S$ powder standards. Although we also attempted to synthesize $Li_2S_4$ powder, it could not be isolated, because it is thermodynamically unstable.[27,40] Since the XANES features of $Na_2S_4$(27, 28) are similar to the predicted features of lithium polysulfides,[29] it is a suitable reference for a qualitative analysis.

Quantitative analysis of XANES data was attempted using a linear combination analysis procedure, but it was not possible to obtain a good fit for all the spectra due to distorted XANES features in many of our *operando* and reference spectra. These distortions can be explained by self-absorption of the X-rays, a common problem seen with sulfur samples.[32,41–43] It is not possible to correct the distortions in *operando* spectra, in which neither the species nor their concentrations are known,[28,43] and therefore, no self-absorption corrections were applied. In principle, self-absorption effects can be eliminated by diluting the amount of sulfur in the sample and reducing the size of the sulfur particles below 1 μm.[43] We illustrate this possibility by characterizing a dilution series of sub-micrometer sized sulfur in our $S_8$/C composite and a dilute liquid sample of sulfur in the DOL-DME solvent (4 mM $S_8$ or 32 mM sulfur). The resulting spectra of the initial composite and the composite samples diluted with Vulcan carbon to 10, 5, 1, 0.5, and 0.1 wt% of sulfur are presented in Figure 2a, while the dilute liquid sample of sulfur is compared to 0.1 wt% $S_8$/C sample in Figure 2b. The figures demonstrate that the sulfur XANES feature remains distorted when the concentration of sulfur is at 1 wt% or higher. Since the concentration of sulfur in carbon-based composites or electrodes is always much higher than 1 wt% in Li-S batteries, and since the polysulfide equilibria are known to be concentration dependent,[11] it was not practical to aim to completely avoid self-absorption effects in the *operando* experiments. Such efforts would lead to a system, which would not be representative of a real battery cell. Consequently, we used a typical sulfur composite with 67 wt% of sulfur and focused on the qualitative interpretation of the *operando* XANES measurements.

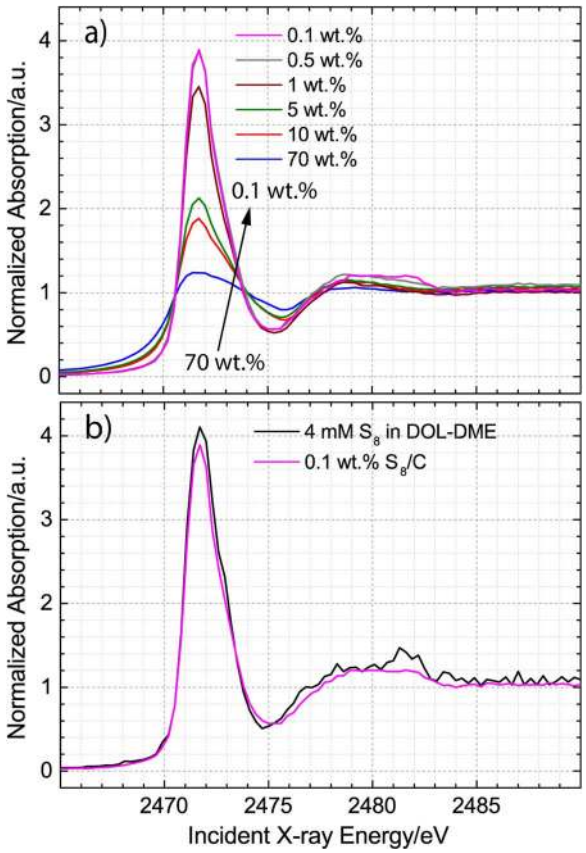


**Figure 2.** a) Normalized sulfur K-edge XANES spectra of the as-prepared $S_8$/C composite (67 wt% sulfur) and $S_8$/C composite diluted with Vulcan carbon to 10, 5, 1, 0.5, and 0.1 wt% of sulfur. Distortions in the spectrum are present at 1 wt% sulfur and higher concentrations; b) XANES spectrum of 4 mM $S_8$ dissolved in DOL-DME compared to the spectrum of $S_8$/C composite diluted to 0.1 wt% of sulfur. Neither sample contains self-absorption distortions.

## Results and Discussion

*Benchmarking of electrochemical performance.*— The electrochemical performance of the *operando* cell was benchmarked against a Swagelok T-cell in a standard electrolyte, consisting of 1 M LiTFSI and 0.5 M $LiNO_3$ dissolved in DOL-DME (1:1 vol:vol), using discharge and charge current of 167 mA/$g_s$ (i.e., a C-rate of 0.1 $h^{-1}$). Owing to the identical electrode configuration in the Swagelok cell (red) and in our *operando* cell (blue), the discharge and charge curves are similar in both cells (Figure 3a). Although only one representative curve is shown, the *operando* cell could reproducibly achieve a first discharge capacity of ca. 1100–1300 mAh/$g_S$ and subsequently charge, thus matching the performance of a standard Li-S cell and approaching the theoretical capacity of Li-S chemistry.

Additional benchmarking experiments were also performed in two other electrolytes, which were subsequently used in the *operando* XANES experiments: 1 M $LiClO_4$ and 0.5 M $LiNO_3$ dissolved in DOL-DME and 1 M $LiClO_4$ and 0.5 M $LiNO_3$ dissolved in DMAC. Because *operando* experiments focused on the discharge mechanism, only the discharge curves are shown in Figures 3b and 3c. The two figures demonstrate that during XANES characterization the replacement of LiTFSI with $LiClO_4$ does not have a significant effect on the reduction potentials of the high and low voltage plateaus, while the replacement of the low dielectric DOL-DME solvent with the high dielectric DMAC solvent results in the predicted shifts in the OCV and the reduction potentials due to substantially different $Li^+$ solvation energies in the two types of electrolyte solvents.[14,44]

The successful electrochemical benchmarking of our *operando* cell indicates that it has unique capabilities. Other published or commercially available spectro-electrochemical cell designs are unable to achieve both standard electrochemical performance and make all three components of the cell available to spectroscopic characteri-

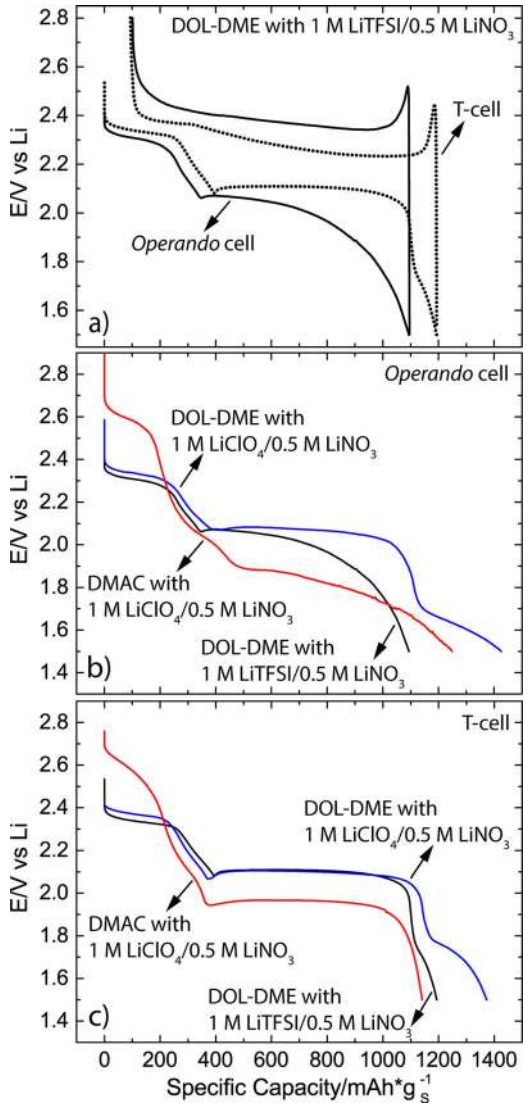


**Figure 3.** a) Comparison of discharge and charge curves at a C-rate of 0.1 $h^{-1}$ obtained in the T-cell and in the *operando* cell in a standard electrolyte, consisting of 1 M LiTFSI and 0.5 M $LiNO_3$ dissolved in DOL-DME mixture. b), c) Comparison of the discharge curves in three different electrolytes (1 M LiTFSI and 0.5 M $LiNO_3$ dissolved in DOL-DME, 1 M $LiClO_4$ and 0.5 M $LiNO_3$ dissolved in DOL-DME, and 1 M $LiClO_4$ and 0.5 M $LiNO_3$ dissolved in DMAC) in the *operando* cell b) and the T-cell c).

zation. The most common cell design employed with Raman, X-ray photo-electron and XANES spectroscopies relies on a modification to a current collector of a coin, pouch, or Swagelok cell through an introduction of a window compatible with the desired technique.[27,28,45,46] In this setup, the excellent electrochemical performance of the cell is maintained, but it is only possible to measure a sum signal of the electrode and the electrolyte found in the pores of the electrode. Another cell design has followed a different strategy by pressing the entire surface area of both electrodes, in a side-by-side arrangement, against the window material.[47,48] Such design enables spectroscopic access to each of the two electrodes and the separator, but only at the expense of poor electrochemical performance.[47] Hence, the capability of the presented *operando* cell design to maintain a favorable electrode configuration and therefore, standard electrochemical performance, while simultaneously exposing the two electrodes and the separator to the X-rays, is a significant improvement over the commercially available and previously published spectro-electrochemical cell designs.

*Validation of operando characterization of intermediates.*— The *operando* discharge curves for the DMAC and DOL-DME cells are presented in Figures 4a and 4c, both as a function of cell capacity and of the number of consumed $e^-/S_8$. They demonstrate the expected high and low voltage plateaus and typical discharge capacities of 12–13 $e^-/S_8$ (1250–1350 mAh/$g_s$). The *operando* XANES spectra were collected continuously, with each spectrum lasting either 9 (DMAC) or 8 (DOL-DME) minutes, which corresponded to a discharge interval of 0.24 $e^-/S_8$ (25 mAh/$g_s$) in DMAC and 0.22 $e^-/S_8$ (23 mAh/$g_s$) in DOL-DME. To verify that our cell design could provide accurate information on the composition of intermediates, we first focused on the XANES spectra obtained in the well characterized 0–4 $e^-/S_8$ initial discharge region.

To interpret the XANES spectra we relied on three standards: $S_8$, $S_4^{2-}$ polysulfide, and $Li_2S$. The XANES spectra of $S_8$ and $Li_2S$ were measured using commercially available powders, while the spectrum of $S_4^{2-}$ polysulfide was approximated by the spectrum of a synthesized $Na_2S_4$ powder. Although the spectra of other polysulfides such as $S_3^{2-}$, $S_5^{2-}$, $S_6^{2-}$, $S_8^{2-}$ are not presented in this study, the positions of their XANES features are expected to be well represented by the spectrum of $S_4^{2-}$ polysulfide.[27–29] This is rationalized by a computational study, which has demonstrated that the charge on a polysulfide chain migrates toward the two terminal sulfur atoms.[29] This phenomenon leads to a sulfur K-edge XANES signal consisting of two features, with the first feature at ~2470–1 eV corresponding to the negatively charged terminal sulfur atoms and the second feature at ~2472–3 eV corresponding to the uncharged ('neutral') internal sulfur atoms. As the length of the polysulfide chain decreases, the absolute energy position of each feature experiences little change, while the intensity ratio between the second and the first peak decreases. The spectra of various polysulfides can thus be differentiated by the relative intensities or areas of the two peaks.[29] During *operando* characterization, however, $S_8$ and many different polysulfides can be present simultaneously, which makes quantitative analysis of the relative concentrations of the polysulfides difficult, if not impossible.

The spectra of the references are shown in Figure 5 and demonstrate the expected characteristics of $S_8$,[46] polysulfides,[29] and $Li_2S$.[27,29] Specifically, $S_8$ has a single major peak at 2472 eV, $S_4^{2-}$ has two major peaks at 2470 eV and 2472 eV, and $Li_2S$ has two major peaks at 2473 eV and 2475.5 eV and an additional feature at 2483 eV. Although $Li_2S$ is in a more reduced state than $S_8$ and polysulfides, the presence of its main features in the 2473–2475.5 eV region can be explained by the ionic character of the $Li_2S$ bond.[49] In our qualitative analysis we will identify formation of polysulfides by the appearance of the 2470 eV feature and the formation of $Li_2S$ by the appearance of a convex feature at 2475.5 eV (Figure 5). The slightly dampened shape of all the peaks indicates the presence of self-absorption, which can be explained by the use of manual grinding procedure and the resulting micrometer-sized and not the needed sub-micrometer-sized particles and/or slightly too high amount of the sulfur compound used.[41] In the inset of the figure, we also include the spectrum of 4 mM $S_8$ in DOL-DME to compare a sample without any self-absorption distortions to our three standards. The observed presence of the self-absorption artifact does not restrict qualitative interpretation of the *operando* XANES spectra, which, as has been previously explained, also experiences self-absorption problems.

Figures 4b and 4d show the *operando* XANES spectra collected immediately prior to the beginning of the discharge (0 $e^-$) and after a consumption of 1, 2, 3, and 4 $e^-/S_8$ in reaction 1. From the XANES spectra corresponding to 0 $e^-/S_8$, which are characterized by a major peak at an incident X-ray energy of 2472 eV and match the self-absorbed spectrum of the $S_8$ reference in Figure 5, it can be concluded that only $S_8$ is present in the DMAC and DOL-DME *operando* cells after the initial OCV period of 1.5–2 hours. As the discharge proceeds, a new feature appears at an incident energy that is approximately 2 eV lower than the main feature of $S_8$, indicating reduction of $S_8$ to polysulfides. Subsequently, the absorption intensity of the newly acquired feature grows as the number of the transferred electrons increases from 1 $e^-/S_8$ to 4 $e^-/S_8$, while, at the same time, the absorption

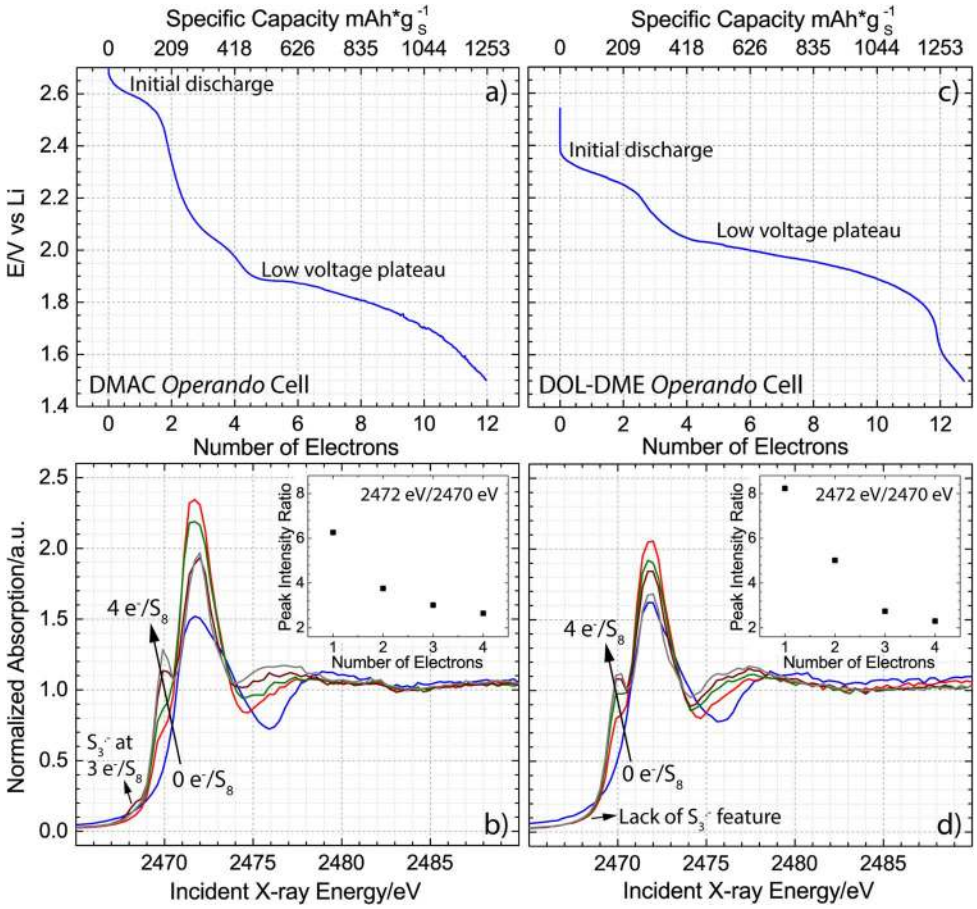


**Figure 4.** *Operando* discharge curve in a) DMAC and c) DOL-DME cells plotted both as a function of the number of electrons consumed in $S_8$ + 16 Li + 16 $e^-$ → 8 $Li_2S$ reaction and as a function of specific capacity (at a C-rate of 0.1 $h^{-1}$). Normalized o*perando* sulfur K-edge XANES spectra obtained in the well-characterized 0–4 $e^-/S_8^-$ discharge region of the b) DMAC and d) DOL-DME cells, with the inset graphics visualizing the ratio between the two polysulfides peaks at 2472 eV and 2470 eV. To estimate the peak intensity of the feature at 2470 eV, a background subtraction was performed using the normalized absorption values of the 0 $e^-/S_8$ spectrum in the 2469–2471 eV region and the resulting value at 2469.9 eV was used as the peak intensity. The intensity of the peak at 2472 eV corresponds to the normalized absorption at 2472 eV.

intensity of the main feature at 2472 eV either decreases or remains constant. These changes are visualized in the insets of Figures 4b and 4d by plotting the ratio of the peak intensities located at 2472 eV and 2470 eV as a function of transferred electrons (1–4 $e^-/S_8$).

As discussed in the introduction, the discharge mechanism in the 0–4 $e^-/S_8$ region in the high dielectric DMAC electrolyte is expected to be different from the discharge mechanism in the low dielectric DOL-DME electrolyte. In particular, previous UV-Vis spectroscopy studies have shown that the $S_3^{\bullet-}$ appears in high but not low dielectric solvents,[11] and that its concentration reaches a maximum after a charge transfer of 2.7 $e^-/S_8$.[15] Recently, a unique XANES feature of the $S_3^{\bullet-}$ has been identified by Fleet and Liu[30] and confirmed by Cuisinier et al.[31] This feature corresponds to 1s → 3p(π∗) transition of the unpaired electron and manifests as an additional signal in the 2468–2469 eV region of a typical polysulfide spectrum.[30] A close inspection of the XANES spectra in Figure 4 reveals that an additional shoulder is present in the spectra of the DMAC *operando* cell at a discharge of 3 $e^-/S_8$. Consequently, we used the observed feature of the $S_3^{\bullet-}$ to assess the ability of our *operando* cell to track polysulfide intermediates.

To compare our *operando* results to the previous UV-Vis spectroscopy studies, we examined the signal at 2468–2469 eV in both DMAC and DOL-DME in the 2.0–4.2 $e^-/S_8$ region of the discharge curves (Fig. 6). In the DMAC cell (Figs. 6a and S2) a new XANES feature, which manifests as a shoulder at ∼2468.4 eV, becomes prominent after a charge transfer of 2.3 $e^-/S_8$. This feature subsequently reaches a maximum after a charge transfer of 2.5–2.8 $e^-/S_8$ and then decreases gradually, until 4.2 $e^-/S_8$ are transferred. These results closely match the UV-Vis spectroscopy results of Bonnaterre and Cauquis[15] and are in excellent agreement with the initial reduction mechanism of $S_8$ summarized by reactions 2–4, but they disagree with the recent work of Cuisinier et al., which claims that the intensity of $S_3^{\bullet-}$ signal peaks at 3.2 $e^-/S_8$ (340 mAh/$g_s$) and persists until 8.1 $e^-/S_8$ (850 mAh/$g_s$) in the same electrolyte.[31] The differences in the development of $S_3^{\bullet-}$ intensities presented in this work and in the work of Cuisinier et al. can be explained by an interruption to the discharge that occurred in the work of Cuisinier et al.[31] The interruption occurred after a discharge of ∼2.7 $e^-/S_8$ and lasted 2 hours. Although no additional discharge occurred in this period, the disproportionation reactions continued to take place, which must have led to significant changes in the relative concentrations of the intermediates. These considerations explain why the intensities of the XANES features reported by Cuisinier et al. are not representative of the intermediates that form during a standard discharge and cannot be reliably associated with a particular discharge capacity. In the DOL-DME cell (Figs. 6b and S2), the spectra are featureless in the same 2468–2469 eV region, indicating the lack of $S_3^{\bullet-}$ formation in the low dielectric solvent. This result is consistent with the absence of features in the 2468–2469 eV region in all previous *operando* XANES studies that used low dielectric solvents (e.g., in DOL-DME[27,31,32,34] and TEGDME,[35] even though the authors of the latter study incorrectly interpreted the feature at 2470 eV to correspond to the $S_3^{\bullet-}$). The successful observation of $S_3^{\bullet-}$ intermediate in high

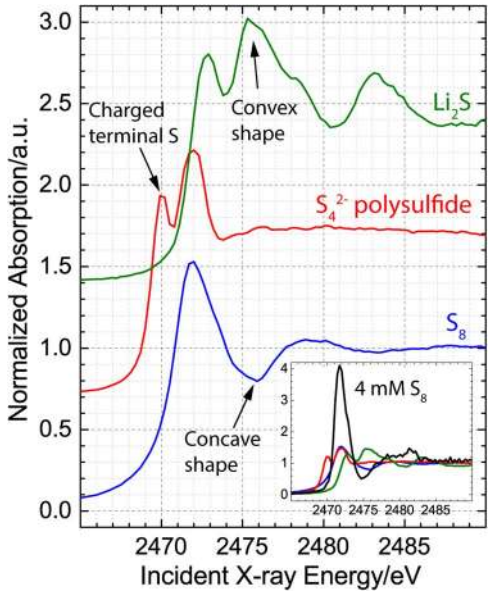


**Figure 5.** Normalized sulfur K-edge spectra of three standards: $S_8$, $S_4^{2-}$ polysulfide, and $Li_2S$. The spectrum of $S_4^{2-}$ polysulfide was obtained using $Na_2S_4$ powder. To clearly display the differences in the features of the three species the spectra of $S_4^{2-}$ polysulfide and $Li_2S$ are offset by 0.7 and 1.4 units, respectively. Because the standards demonstrate some self-absorption distortions, the inset compares the undistorted spectrum of 4 mM $S_8$ in DOL-DME to the spectra of the three standards. In our analysis, formation of polysulfides is identified by the appearance of the peak at ∼2470 eV, which corresponds to the charged terminal sulfur atoms, while formation of $Li_2S$ product is identified by the formation of a peak at ∼2475.5 eV. At 2475.5 eV the spectrum of $Li_2S$ has a clear convex shape, the spectrum of the polysulfide does not have a significant feature, and the spectrum of $S_8$ has a concave shape.

but not low dielectric solvent at the predicted number of discharged electrons confirms the ability of our cell to reliably track polysulfide intermediates and verifies the spectroscopic capabilities of our cell.

*Detection of $Li_2S$ formation in the low-voltage plateau.*— Having validated our experimental method in the well characterized 0–4 $e^-/S_8$ initial discharge region, we now extend it to the less characterized low voltage discharge plateau (4–12 $e^-/S_8$) to understand the dependence of discharge products formation on the strength of the ion-solvation properties of the environment. If the electro-reduction mechanism were strictly sequential, after 8 $e^-/S_8$ are discharged in reaction 1, $S_8$ would be entirely converted to $Li_2S_2$ intermediate (reaction 7). During the subsequent discharge steps, $Li_2S_2$ could be reduced to $Li_2S$ as shown in reaction 8.

$$S_8 + 8\,e^- + 8\,Li^+ \rightleftharpoons 4\,Li_2S_2 \quad [7]$$

$$4\,Li_2S_2 + 8\,e^- + 8\,Li^+ \rightleftharpoons 8\,Li_2S \quad [8]$$

Alternatively, during a simultaneous electro-reduction process, which allows reactions 7 and 8 to occur in parallel,[22] or as a result of a disproportionation mechanism proposed by Lu et al.,[14] $Li_2S$ could form earlier in the discharge, before 8 $e^-/S_8$ are consumed. To understand how the nature of the intermediates changes during the discharge in the low voltage plateau, we examine the spectra that were collected in DMAC and DOL-DME cells, as the extent of discharge increased from 4 $e^-/S_8$ to 12 $e^-/S_8$. We note that because the applied potential in the 4–12 $e^-/S_8$ discharge region is below 2.1 V vs. Li in the DOL-DME cell and 1.8 V in the DMAC cell, we do not consider $S_8$ reduction as a possible contribution to the changes seen in the XANES feature at 2472 eV. At these potentials $S_8$ would either rapidly reduce, as was previously demonstrated using RRDE characterization,[14] or remain present as electrically isolated species.

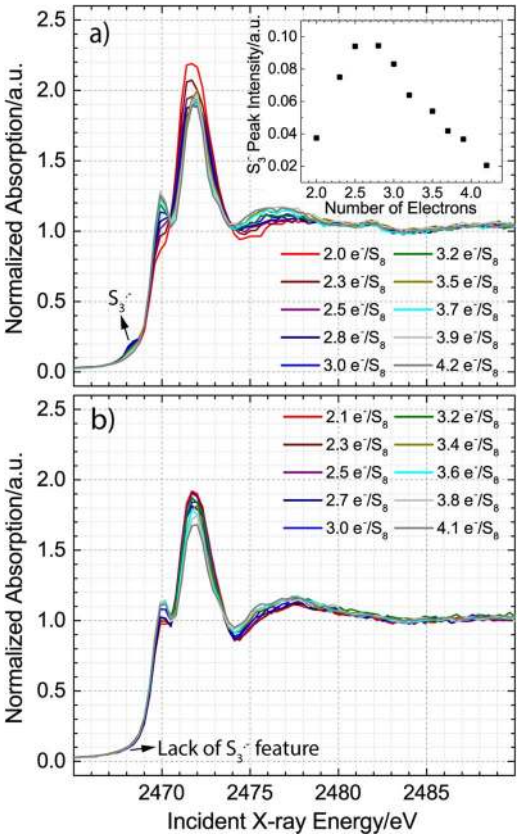


**Figure 6.** a) Normalized *operando* sulfur K-edge XANES spectra demonstrating the observation of $S_3^{\bullet-}$ intermediate in the 2.0–3.9 $e^-/S_8$ region of the DMAC cell with an inset graphic visualizing the peak intensity of the $S_3^{\bullet-}$ feature. The peak intensity was determined by subtracting the spectrum collected after a discharge of 1.3 $e^-/S_8$, in which no feature was present in the 2468–2469 eV region, and reporting the peak maximum of each spectrum. b) Normalized *operando* sulfur K-edge XANES spectra demonstrating the lack of formation of $S_3^{\bullet-}$ intermediate in the 2.1–4.1 $e^-/S_8$ region of the DOL-DME cell.

Figure 7a shows five spectra corresponding to discharge states after 4, 6, 8, 10, and 12 $e^-/S_8$ are transferred in the DMAC cell. All five spectra contain the polysulfide peak at 2470 eV. This polysulfide signature feature and its accompanying main peak at 2472 eV decrease in intensity as the extent of discharge increases, which indicates that the overall proportion of polysulfides inside the battery is decreasing. The $Li_2S$ feature at 2475.5 eV is prominent after a discharge of 6–12 $e^-/S_8$, but a small convex peak can already be seen after a discharge of 4 $e^-/S_8$. To clarify the onset of $Li_2S$ formation, we examine five *operando* spectra collected in the DMAC electrolyte solvent in the 2–6 $e^-/S_8$ discharge region in Figure 7b. After a discharge of 2–3 $e^-/S_8$ the shape of the feature at 2475.5 eV is still concave, indicating that little to no $Li_2S$ is present in the cell. As the extent of discharge increases to 4–5 $e^-/S_8$, however, the feature at 2475.5 eV becomes convex. This observed change in the peak shape provides direct evidence that $Li_2S$ is present in the cell after a discharge of 4–5 $e^-/S_8$.

To determine if there is a difference in the observed onset of $Li_2S$ formation between DMAC and DOL-DME cells, Figure 7c shows five *operando* spectra corresponding to the 4–12 $e^-/S_8$ discharge region of the DOL-DME cell. As in the DMAC cell, all spectra contain the polysulfide feature at 2470 eV and a growing signal at 2475.5 eV. Unlike the DMAC cell, the main polysulfide peak at 2472 eV is less prominent in the DOL-DME cell and after an electron transfer of only 8 $e^-/S_8$ decreases to a normalized absorption intensity value that is below the value of the $Li_2S$ feature at 2475.5 eV. Additionally, two extra features are seen in the DOL-DME spectra at 2478 eV and 2482 eV. These features correspond to beam-induced oxidation

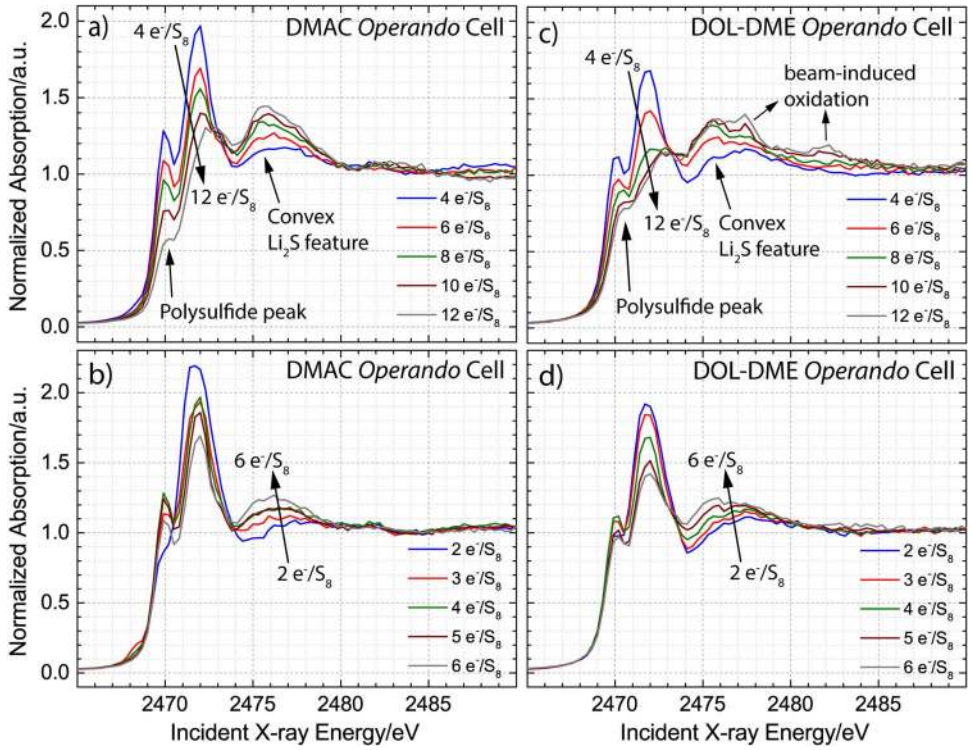


**Figure 7.** Examination of low voltage plateau intermediates using five normalized *operando* sulfur K-edge XANES spectra in a) DMAC and c) DOL-DME cells corresponding to 4, 6, 8, 10, and 12 $e^-/S_8$. Identification of approximate onset of $Li_2S$ formation using five normalized *operando* sulfur K-edge XANES spectra in b) DMAC and d) DOL-DME cells corresponding to 2, 3, 4, 5, and 6 $e^-/S_8$. The figure demonstrates that the formation of $Li_2S$ begins at 4–5 $e^-/S_8$ in both types of cells.

of sulfur species (Figure S1) and are not related to the discharge mechanism. The signal at 2475.5 eV has a clear contribution from $Li_2S$ spectrum after an electrochemical transfer of 6–12 $e^-/S_8$, indicating that $Li_2S$ appears near the beginning of the low voltage plateau. To clarify the onset of $Li_2S$ formation, Figure 7d examines five *operando* spectra collected in the DOL-DME cell in the 2–6 $e^-/S_8$ discharge region. In similarity to the spectra obtained in the DMAC cell, DOL-DME spectra collected after an electrochemical transfer of 2–3 $e^-/S_8$ have a concave shape at 2475.5 eV and thus, contain little to no $Li_2S$. As the extent of discharge increases to 4 $e^-/S_8$ the feature transitions from a concave to a convex shape, while a further increase in the number of electrons transferred to 5–6 $e^-/S_8$ leads to a formation of a clear convex peak. These observed transformations in the shape of the XANES feature at 2475.5 eV indicate that the onset of $Li_2S$ formation in the DOL-DME cell occurs at a similar point of the discharge as in the DMAC cell (4–5 $e^-/S_8$). The identified formation of $Li_2S$ after a discharge of 4–5 $e^-/S_8$ (420–520 mAh/$g_s$) in both cells confirms that $Li_2S$ coexists with polysulfides at the beginning of the low-voltage plateau, as has been previously suggested by XRD[20] and electrochemical impedance spectroscopy,[21] and provides direct evidence against the sequential reduction mechanism, in which $Li_2S$ is expected to form only after all of $S_8$ is reduced to $Li_2S_2$.

Interestingly, previous *operando* XANES studies have not demonstrated $Li_2S$ formation at such an early point of the discharge using standard electrolyte and electrode formulations. In one study, which reported both ex situ and in situ sulfur K-edge XANES spectra in a sulfolane solvent with 1 M LiTFSI salt, formation of $Li_2S$ was detected only at the very end of the discharge.[28] In a different study, which used a DOL-DME solvent with 1 M $LiClO_4$ and 0.5 M $LiNO_3$, $Li_2S$ was found to appear in the middle of the low-voltage plateau at a discharge capacity of 700–800 mAh/$g_s$ (6.7–7.7 $e^-/S_8$).[27] Finally, in two very recent studies, which characterized the discharge behavior of both a standard Li-S battery based on the DOL-DME electrolyte solvent and $S_8$/C composite and a battery employing either a new electrolyte[32] or a new type of electrode,[34] $Li_2S$ formation was demonstrated to occur as early as 250–320 mAh/$g_s$ (2.3–3.0 $e^-/S_8$) in the novel systems, but a lack of $Li_2S$ was reported at the beginning of the low-voltage plateau in the standard cells.[32,34] Specifically, the authors either demonstrated an absence of $Li_2S$ contribution to sulfur K-edge XANES at 450 mAh/$g_s$[34] or detected an onset of $Li_2S$ formation at 1000 mAh/$g_s$.[32] While the exact reason for the higher sensitivity of our *operando* cell to the detection of $Li_2S$ is not known, it may be related to its unique measurement geometry.

Having established that the onset of $Li_2S$ formation occurs at the beginning of the low-voltage plateau in both cells, we examine in detail the observed differences in the spectra of the two cells after an electrochemical transfer of 8 $e^-/S_8$. Figure 8 directly compares the spectra obtained in the DMAC and DOL-DME cells after a discharge

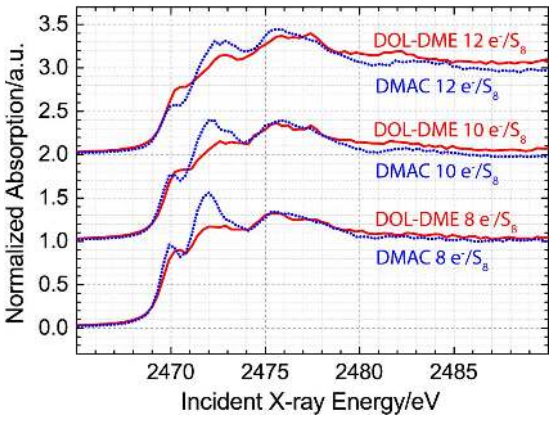


**Figure 8.** Comparison of the normalized *operando* sulfur K-edge XANES spectra in DMAC and DOL-DME cells collected after an electrochemical transfer of 8, 10, and 12 $e^-/S_8$. The spectra corresponding to a discharge of 10 and 12 $e^-/S_8$ are offset by 1.0 and 2.0 units, respectively.

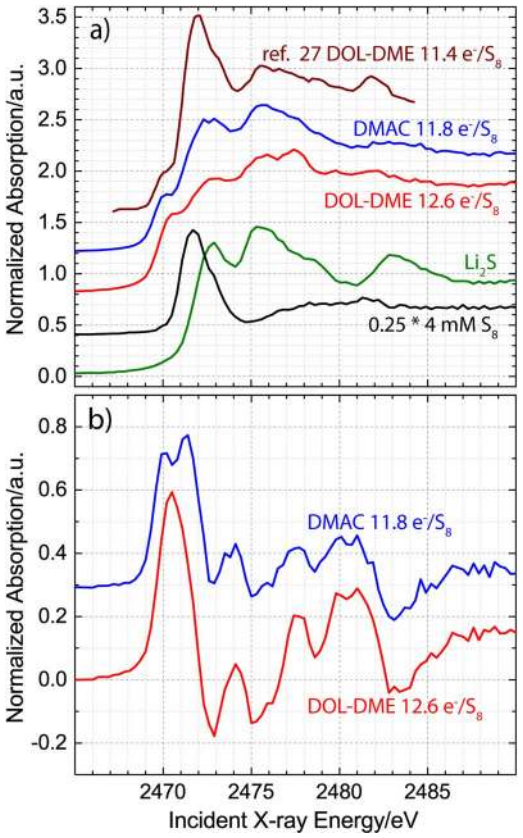


**Figure 9.** a) Comparison of $Li_2S$ and 4 mM $S_8$ reference spectra to the literature results from Ref. 27 and the normalized *operando* sulfur K-edge XANES spectra collected at the very end of discharge in DMAC and DOL-DME cells. To facilitate comparison of the spectra, the incident X-ray energy of the spectrum from ref. 27 is calibrated to the same energy scale by shifting it to a higher X-ray energy by 2.2 eV, the spectrum of 4 mM $S_8$ is multiplied by 0.25, and the spectra of 4 mM $S_8$, DOL-DME, DMAC, and ref. 27 are offset by 0.4, 0.8, 1.2, and 1.6 units, respectively. The extent of the electrochemical discharge corresponds to 11.4 $e^-/S_8$ in ref. 27 and to 11.8 $e^-/S_8$ and 12.6 $e^-/S_8$ in our DMAC and DOL-DME cells. b) Normalized sulfur K-edge XANES spectra corresponding to the difference between the last spectrum obtained in the two cells and the $Li_2S$ reference spectrum.

of 8, 10, and 12 $e^-/S_8$. It clearly demonstrates that at a discharge state of 8 $e^-/S_8$ the $Li_2S$ feature at 2475.5 eV is the main feature in the DOL-DME cell, while the polysulfide features at 2472 eV and 2470 eV are the main features in the DMAC cell. As the number of transferred electrons increases to 10 and then 12 $e^-/S_8$, the normalized absorption intensity in the 2470–2472 eV region continues to decrease, while the XANES signal from $Li_2S$ product becomes more prominently seen at 2473 eV, where a second $Li_2S$ peak is expected. In particular, in the DMAC cell the polysulfide feature at 2472 eV decreases until its intensity is about equal to the intensity of the peak at 2473 eV, while in the DOL-DME cell the intensity of the polysulfide feature drops below the intensity of the peak at 2473 eV. These observed differences in the DOL-DME and DMAC spectra in the 8–12 $e^-/S_8$ discharge region indicate a smaller relative proportion of polysulfides in the DOL-DME cell and suggest that the disproportionation of polysulfides in a poorly ion-solvating environment of DOL-DME solvent is more rapid than in the strongly ion-solvating environment of DMAC solvent.

Previous *operando* XANES studies have demonstrated a surprising presence of unreacted $S_8$ at the end of the discharge of Li-S battery.[27,28,33] To determine if our tested cells also have $S_8$ at the end of discharge, which, for example, could have been electrically isolated from the cathode and therefore, remained in an unreacted oxidized form, Figure 9a compares the final spectra obtained in DMAC and DOL-DME cells to the previous literature results of Cuisinier et al.[27] In disagreement with previous results, we do not see a significant feature at 2472 eV in either cell, suggesting that when our *operando* cells reach the end of the discharge, little to no $S_8$ is present. To better understand the type of species that are present in the last spectra, we subtract $Li_2S$ features from each spectrum and visualize the difference spectra in Figure 9b. Inspection of the subtracted XANES spectrum of the DMAC cell (blue spectrum in Fig. 9b) reveals the presence of polysulfide species, while inspection of the subtracted XANES spectrum of the DOL-DME cell (red spectrum in Fig. 9b) reveals a component that does not correspond to a typical polysulfide spectrum, but rather has a single broad feature at 2470.5 eV. The presence of a species with a feature at 2470.5 eV has also been previously detected in an ex situ XANES spectrum by Patel et al., who have postulated that it corresponds to a different form of $Li_2S$.[28] We hypothesize that the feature corresponded not to $Li_2S$ but to $S_2^{2-}/Li_2S_2$, based on the first-principles calculations of Pascal et al.,[29] who have shown that $S_2^{2-}/Li_2S_2$ is expected to have a lone peak at an energy that is approximately 0.5 eV more positive of the original polysulfide feature.

The observed differences in the final composition of species in DMAC and DOL-DME cells suggest that different mechanisms may contribute to reaching the end of discharge in the two different ion-solvating environments. In the strongly ion-solvating environment of the DMAC cell, a possible explanation for reaching the end of the discharge at only 12 $e^-$ out of possible 16 $e^-/S_8$ is that as the lower order polysulfides are depleted, they become more stabilized in the reduced form and do not readily disproportionate to $Li_2S$ and either a higher order polysulfide or $S_8$ (reactions 5 and 6). Their increased stability leads to an increase in the applied overpotential necessary to maintain the prescribed discharge current and the subsequent end of the discharge. In the poorly ion-solvating environment of the DOL-DME cell, the change in the stability of the lower order polysulfides cannot play a similar role in reaching the end of the discharge, because almost all of the lower order polysulfides are consumed after a charge transfer of only 10 $e^-/S_8$. It is possible, however, that the hypothesized formation of $S_2^{2-}/Li_2S_2$ intermediate could be contributing to the inability of the cell to extract more than 12.6 $e^-/S_8$. For example, if the $S_2^{2-}/Li_2S_2$ intermediate cannot be further electro-reduced or disproportionated, the conversion of all other species in the cell to $S_2^{2-}/Li_2S_2$ and $Li_2S$ will eventually lead to a premature end of the discharge (Figure 4c).

## Conclusions

In this work, we introduce a new spectro-electrochemical cell design with unique characterization features. Typical *operando* cell designs offer either a proper electrochemical performance through a modification of a coin, pouch, or Swagelok cell or provide advanced spectroscopic capabilities, such as spectroscopic access to the electrodes and the separator for spatially-resolved measurements, but not both qualities at the same time. In contrast, our cell combines both excellent electrochemical performance, as has been demonstrated in the benchmark tests using a standard Swagelok T-cell, and offers the possibility to characterize different cell components by pressing the edges of the electrodes and the separator against the X-ray window. Although in this study we use a defocused beam and do not perform spatially-resolved measurements, we successfully confirm the spectroscopic capabilities of the cell by tracking the formation of $S_3^{\bullet-}$ intermediate and closely matching the previously reported UV-Vis spectroscopic results.

After establishing the spectro-electrochemical capabilities of our *operando* cell, we subsequently use it to investigate the influence of the solvent on the conversion of polysulfides to $Li_2S$ by employing cells built using DMAC and DOL-DME electrolyte solvents. In good agreement with previous XRD, electrochemical impedance spectroscopy, and modeling studies, we observe the formation of $Li_2S$ after a discharge of only 4–5 $e^-/S_8$ in both types of cells, which represents the earliest *operando* XANES detection of $Li_2S$ using standard electrolyte and electrode formulations. Furthermore, by offering simultaneous detection of liquid and solid intermediates, our experiments highlight the advantages of *operando* XANES over other characterization

approaches, including UV-Vis spectroscopy, HPLC, and XRD, which can detect either polysulfides or $Li_2S$ but not both species at the same time.

Additional analysis of the XANES spectra reveals that despite a similar initial onset of $Li_2S$ formation in the two cells, subsequent conversion of polysulfides to $Li_2S$ is found to be more rapid in the DOL-DME than in the DMAC cell. Furthermore, at the end of the discharge, two different compositions are observed in the two cells. In the DMAC cell, we detect the presence of $Li_2S$ and a polysulfide intermediate, while in the DOL-DME cell, we detect the presence of $Li_2S$ and what likely is a $S_2^{2-}$/$Li_2S_2$ intermediate. In disagreement with previous studies, the final spectra do not indicate significant presence of $S_8$ in either type of the cell. Taken as a whole, the observed differences between the *operando* XANES results obtained in the DMAC and in the DOL-DME cells provide strong evidence that the disproportionation steps are faster in a poorly rather than a strongly ion-solvating environment, which, as has been recently proposed by Lu et al.,[14] can explain the higher rate capabilities of Li-S batteries based on low dielectric solvents, such as DOL-DME.

## Acknowledgments

The described sulfur K-edge XANES measurements were performed at the PHOENIX beamline at Swiss Light Source, Paul Scherrer Institut, Villigen, Switzerland. The authors also thank Diamond Light Source, Didcot, UK for access to beamline I18 (SP 8734) that contributed to the results presented here, Konstantin Ignatyev for support during experiments at Diamond Light Source, Anna Eberle and Judith Martin for assessing the discharge behavior of Li-S battery in electrolytes based on $LiClO_4$, LiTFSI, and other salts, and Marc Schönberger and Erik Faber for technical support in designing and building the *operando* cell. Portions of the research leading to these results have received funding from the European Community's Seventh Framework Programme (FP7/2007–2013) under agreement No. 312284 and from the German Ministry of Education and Research (BMBF) under agreement No. 03X4627A. Yelena Gorlin gratefully acknowledges the Alexander von Humboldt Foundation for her Postdoctoral Fellowship. Authors Yelena Gorlin and Armin Siebel contributed equally to this work.

## References

1. M. Z. Jacobson, *Energ. Environ. Sci.*, **2**, 148 (2009).
2. Global EV Outlook: Understanding the Electric Vehicle Landscape in 2020, International Energy Agency (2013).
3. EV Everywhere: Grand Challenge Blueprint, US Department of Energy (2013).
4. K. G. Gallagher, S. Goebel, T. Greszler, M. Mathias, W. Oelerich, D. Eroglu, and V. Srinivasan, *Energ. Environ. Sci.*, **7**, 1555 (2014).
5. B. Scrosati and J. Garche, *J. Power Sources*, **195**, 2419 (2010).
6. P. G. Bruce, S. A. Freunberger, L. J. Hardwick, and J.-M. Tarascon, *Nat. Mater.*, **11**, 19 (2012).
7. J.-M. Tarascon, *Phil. Trans. R. Soc. A*, **368**, 3227 (2010).
8. Y. V. Mikhaylik, I. Kovalev, R. Schock, K. Kumaresan, J. Xu, and J. Affinito, *ECS Trans.*, **25**, 23 (2010).
9. *Fiscal Year 2013 Annual Progress Report for Energy Storage R&D*, US Department of Energy (2014).
10. L. F. Nazar, M. Cuisinier, and Q. Pang, *MRS Bulletin*, **39**, 436 (2014).
11. R. D. Rauh, F. S. Shuker, J. M. Marston, and S. B. Brummer, *J. Inorg. Nucl. Chem.*, **39**, 1761 (1977).
12. R. D. Rauh, K. M. Abraham, G. F. Pearson, J. K. Surprenant, and S. B. Brummer, *J. Electrochem. Soc.*, **126**, 523 (1979).
13. Y. Jung, S. Kim, B.-S. Kim, D.-H. Han, S.-M. Park, and J. Kwak, *Int. J. Electrochem. Sci.*, **3**, 566 (2008).
14. Y.-C. Lu, Q. He, and H. A. Gasteiger, *J. Phys. Chem. C*, **118**, 5733 (2014).
15. R. Bonnaterre and G. Cauquis, *J. Chem. Soc., Chem. Commun.*, 293 (1972).
16. T. Chivers and I. Drummond, *Inorg. Chem.*, **11**, 2525 (1972).
17. R. P. Martin, W. H. Doub, J. L. Roberts, and D. T. Sawyer, *Inorg. Chem.*, **12**, 1921 (1973).
18. X. Ji and L. F. Nazar, *J. Mater. Chem.*, **20**, 9821 (2010).
19. N. A. Cañas, S. Wolf, N. Wagner, and K. A. Friedrich, *J. Power Sources*, **226**, 313 (2013).
20. S. Walus, C. Barchasz, J.-F. Colin, J.-F. Martin, E. Elkaim, J.-C. Lepretre, and F. Alloin, *Chem. Commun. (Cambridge, U. K.)*, **49**, 7899 (2013).
21. L. Yuan, X. Qiu, L. Chen, and W. Zhu, *J. Power Sources*, **189**, 127 (2009).
22. K. Kumaresan, Y. Mikhaylik, and R. E. White, *J. Electrochem. Soc.*, **155**, A576 (2008).
23. L. A. Huff, J. L. Rapp, J. A. Baughman, P. L. Rinaldi, and A. A. Gewirth, *Surf. Sci.*, **631**, 295 (2015).
24. N. A. Cañas, D. N. Fronczek, N. Wagner, A. Latz, and K. A. Friedrich, *J. Phys. Chem. C*, **118**, 12106 (2014).
25. C. Barchasz, F. Molton, C. Duboc, J.-C. Leprêtre, S. Patoux, and F. Alloin, *Anal. Chem.*, **84**, 3973 (2012).
26. A. Kawase, S. Shirai, Y. Yamoto, R. Arakawa, and T. Takata, *Phys. Chem. Chem. Phys.*, **16**, 9344 (2014).
27. M. Cuisinier, P.-E. Cabelguen, S. Evers, G. He, M. Kolbeck, A. Garsuch, T. Bolin, M. Balasubramanian, and L. F. Nazar, *J. Phys. Chem. Lett.*, **4**, 3227 (2013).
28. M. U. M. Patel, I. Arčon, G. Aquilanti, L. Stievano, G. Mali, and R. Dominko, *ChemPhysChem*, **15**, 894 (2014).
29. T. A. Pascal, K. H. Wujcik, J. Velasco-Velez, C. Wu, A. A. Teran, M. Kapilashrami, J. Cabana, J. Guo, M. Salmeron, N. Balsara, and D. Prendergast, *J. Phys. Chem. Lett.*, **5**, 1547 (2014).
30. M. E. Fleet and X. Liu, *Spectrochim. Acta Part B*, **65**, 75 (2010).
31. M. Cuisinier, C. Hart, M. Balasubramanian, A. Garsuch, and L. F. Nazar, *Adv. Energ. Mat.*, 1401801 (2015).
32. M. Cuisinier, P. E. Cabelguen, B. D. Adams, A. Garsuch, M. Balasubramanian, and L. F. Nazar, *Energ. Environ. Sci.*, **7**, 2697 (2014).
33. J. Gao, M. A. Lowe, Y. Kiya, and H. D. Abruña, *J. Phys. Chem. C*, **115**, 25132 (2011).
34. Q. Pang, D. Kundu, M. Cuisinier, and L. F. Nazar, *Nat. Commun.*, **5**, 4759 (2014).
35. M. A. Lowe, J. Gao, and H. D. Abruna, *RSC Advances*, **4**, 18347 (2014).
36. H. Jha and H. A. Gasteiger, DE Patent No. 102013005082 A1. Munich, Germany: Deutsches Patent- und Markenamt (2014).
37. A. M. Flank, G. Cauchon, P. Lagarde, S. Bac, M. Janousch, R. Wetter, J. M. Dubuisson, M. Idir, F. Langlois, T. Moreno, and D. Vantelon, *Nucl. Instrum. Methods Phys. Res., Sect. B*, **246**, 269 (2006).
38. B. Ravel and M. Newville, *J. Synchrotron Rad.*, **12**, 537 (2005).
39. G. Brauer, *Handbuch Der Präparativen Anorganischen Chemie*, Enke Verlag, Stuttgart (1975).
40. P. T. Cunningham, S. A. Johnson, and E. J. Cairns, *J. Electrochem. Soc.*, **119**, 1448 (1972).
41. G. N. George, M. Gnida, D. A. Bazylinski, R. C. Prince, and I. J. Pickering, *J. Bacteriol.*, **190**, 6376 (2008).
42. I. J. Pickering, R. C. Prince, T. Divers, and G. N. George, *FEBS Lett.*, **441**, 11 (1998).
43. G. Almkvist, K. Boye, and I. Persson, *J. Synchrotron Rad.*, **17**, 683 (2010).
44. H. Schneider, C. Gollub, T. Weiß, J. Kulisch, K. Leitner, R. Schmidt, M. M. Safont-Sempere, Y. Mikhaylik, T. Kelley, C. Scordilis-Kelley, M. Laramie, and H. Du, *J. Electrochem. Soc.*, **161**, A1399 (2014).
45. Y.-C. Lu, E. J. Crumlin, T. J. Carney, L. Baggetto, G. M. Veith, N. J. Dudney, Z. Liu, and Y. Shao-Horn, *J. Phys. Chem. C*, **117**, 25948 (2013).
46. T. Gross, L. Giebeler, and C. Hess, *Rev. Sci. Instrum.*, **84**, 073109 (2013).
47. S. J. Harris, A. Timmons, D. R. Baker, and C. Monroe, *Chem. Phys. Lett.*, **485**, 265 (2010).
48. Y.-L. Ding, B. M. Goh, H. Zhang, K. P. Loh, and L. Lu, *J. Power Sources*, **236**, 1 (2013).
49. M. E. Fleet, *Can. Mineral.*, **43**, 1811 (2005).